NUMERICAL SIMULATION OF A DUSTY PLASMA

Reported by Alexander Church – co investigated with David Shone

SUPERVISOR: M. COPPINS : ASSESSOR R. KINGHAM

ABSTRACT

A 3-D numerical simulation of dusty plasmas is presented to principally investigate shell growth, coulomb coupling parameter variation (henceforth referred to as γ or CCP), crystal structure and how varying charge and mass of dust particles affects the system as a whole.

The system utilises an Euler method approach and models only the electrostatic forces between particles. An intelligent temperature control was used to vary dust particle energies. A series of equally spaced concentric shells, whose surfaces were found to be hexagonally packed, was observed. Through varying the temperature, consequently varying Gamma, a phase transition was observed between 130-190 γ, which is in line with the theoretically predicted 172 phase change boundary [1]. Certain numbers of particles (20, 34, 51, 81, 276, 655 and 2137) created very stable shells where a volume (surface) packing efficiency of 65%±1.2% (89%±6%) was observed. Hexagonally packed volumes (surfaces) have an efficiency of 74% (90%), so only the surface structure is said to be hexagonally packed.

At high particle numbers a transition in structure was observed. The new structure is possibly Hexagonally Close Packed and was observed approximately 10 shells from the edge of the simulation.

TABLE OF CONTENTS

INTRODUCTION

REASONING

The fourth state of matter, plasma, is by far the most abundant form of matter within the universe. Every star, nebula and all the 'empty' space between is permeated by plasmas. This state of matter was first coined 'plasma' by Tonks and Langmuir in 1929 [1] but was first discovered in 1879 by Sir William Crookes [2]. Modern silicon wafer production creates plasmas within the laser etching chambers. These plasmas are, on their own, harmless to the microchips. When 'dusty' plasma crystals form and aggregate together, micrometer sized particulates are created. These can contaminate the ultra pure wafers, as discovered by Gary Selwin of IBM [3]. This leads to a higher failure rate, increased production costs and hence increased cost of the final product. The modern world's economy is driven by the microchip, thus dusty plasmas are not just a matter of interest for astronomers and physicists but impact modern day life. Millions of pounds have been and still are being spent to improve 'clean' rooms where silicon wafer production occurs. Every trace of dust is removed from persons working in these laboratories, yet no matter how careful the screening process, it is the very process of producing the microchips that creates the dusty plasma crystals.

It is of paramount importance to understand how these crystals form and with the advent of nanotechnology, fusion reactors and modern propulsion systems, this will become an ever increasing area of research. The number of papers published in this field is rising exponentially, approximately growing 'e fold' every 3.9 years [4], which demonstrates the increasing interest in this area of research.

BACKGROUND

THE COULOMB COUPLING PARAMETER

The coulomb coupling parameter is the ratio of the dust potential energy (P.E.) to the thermal energy of the dust:

$$\gamma_c = \frac{Z_d^2}{r k_B T_d} \exp\left\{-\frac{r}{\lambda_{De}}\right\}$$

EQUATION 1 : COULOMB COUPLING PARAMETER, WHERE λ_{De} IS THE DEBYE LENGTH FOR AN ELECTRON, Z_dIS THE CHARGE OF A DUST GRAIN AND γ_cIS THE COULOMB COUPLING PARAMETER.

For this project only a basic simulation will be taken into account. Thus no "near wall" effects will be considered and gravity will be ignored, as though the experiment were being undertaken in space. For this reason work on edge effects, such as that investigated by Vasut et Al. [5] will not be applied.

For plasma crystals to form the potential energy of a dust particle due to its surrounding neighbours must by significantly more than its thermal energy $k_B T_d$. By replacing r with $n_j^{-1/3}$ (Number Density) and allowing for quasi-neutrality $Z_i n_i = n_e$ we obtain Equation 2

$$\gamma_i \approx Z_i^{\frac{5}{3}}\gamma_e$$

EQUATION 2 : RELATIONSHIP BETWEEN ION AND ELECTRON COUPLING PARAMETER

Ignoring the Debye shielding, it is clear that as the Coupling parameter increases to the power 5/3 with respect to the charge of the ions, the shielding must be included. The average charge on the dust grains can be of the order 10^4 electron charges [6] thus, the Debye shield is a very valid assumption given the $Z^{5/3}$ coupling parameter relationship.

Thus we are arrive at:

$$\gamma_c = \frac{Z_d^2 n_d^{1/3}}{k_B T_d}\exp\{-\kappa_d\} where\ \kappa_d = \left\{\frac{1}{n_d^{1/3}\lambda_{De}}\right\}$$

EQUATION 3 : COULOMB COUPLING PARAMETER [1]

According to Ikezi [7] if the coupling parameter is greater than 172 then crystallisation should occur.

SELF ORGANISATION

Another interesting aspect of dusty plasmas is the conditions required for self organisation based on plasma density, plasma temperature and the coupling parameter. From Adachi *et al*. [8] the following diagram (Figure 1, below) shows how their 1 dimensional computer simulation was used to show the conditions in which self organisation took place. A further study into how this model can be expanded into 3-D, to check whether these values still hold true, would be of great value when studying dusty plasmas in the real world.

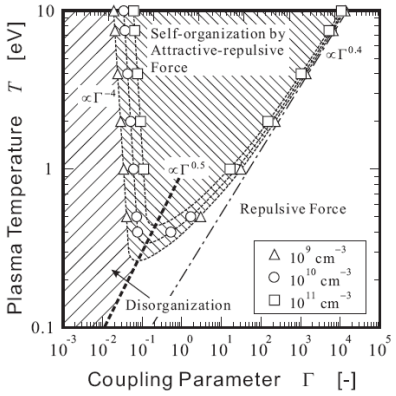

FIGURE 1 : THIS SHOWS HOW THE ATTRACTIVE-REPULSIVE REGION BORDERS WITH THE "REPULSIVE" REGION ALONG THE LINE PROPORTIONAL TO $\Gamma^{-0.4}$ AND BORDERS WITH THE DISORGANISATION REGION ALONG THE LINE PROPORTIONAL TO Γ^{-4}.

The simulation will use a plasma temperature of 2eV and a density of $10^{11}cm^{-3}$. From the above graph the simulation should become disorganised at gamma < 0.1. The crystal should be self organised from any value approximately above 100γ (when ignoring attractive forces).

METHODS

COMPUTATIONAL METHOD

The program was written in Visual Studio C++ including standard libraries. Also used were the GSL Scientific Library [9] and the Glut Open GL Graphics Library [10]. The code is divided into 3 sections.

The first section is a Particle Class which defines all the forces and properties of a particle. Access to all members of the class is done through calling 'get' functions. This class also can switch between spherical polar co-ordinates and Cartesian co-ordinates.

The second section is the Main.cpp which contains all the main coding functions for displaying to screen, file input/output, particle-particle interaction, user interface and all the analysis routines (described later).

The final section of code contains all our global variables, as well as constants such as the charge of an electron. Although it is 'bad' coding practice to have global variables rather than a 'black box' approach, global variables were required so OpenGL could be used. A black box method is where each function is self contained and only requires a set of inputs passed to the function for it to give an output or vary one of the inputs. It is generally considered more robust to coding errors as well as being easier to debug, hence is favoured by programmers. However, due to a lack of practice on how to pass inputs through OpenGL, global variables had to be used to ensure information could be passed between different functions.

PARTICLE INTERACTION

The particle-particle interactions were done for each particle in turn with every other particle. The more efficient box tree [11] process was not used due to time constraints and computational difficulty. To lower the number of calculations if particle A felt a force x from another particle B, then Newton stated that particle B would feel a force –x from Particle A. This reduces the number of calculations by a factor of:

$Effeciency = \frac{1}{n^2}\sum_{i=1}^{n-1} i = \frac{n-1}{2n} = \frac{1}{2} - \frac{1}{2n}$ where n is the number of calculations done per function evaluation.

Thus, if the simulation is run with at least 200 particles the overall efficiency of the method is approximately ½ that of a direct n^2 approach. As explained in 'Time Step Method' an Euler method was used to further reduce calculations. For the errors associated with this method see the 'Errors' section on page 25.

During the simulation at every time step (if the apparatus wall was enabled) all the particle velocities were checked as to whether or not by the next time step their position would be outside the apparatus. If so, a time for collision with the apparatus wall was calculated and time for each particle in turn would be moved to the collision point time. Its deflection and subsequent velocity were calculated and the entire process repeated until h (time step length) had passed. This resulted in some particles 'bouncing' along the wall.

Due to the rarity of particle-particle collisions (low density), only if a collision was detected would the particles be deflected and no 'time loop', as described above, would be used.

TIME STEP METHOD

Time was moved forward by a fixed interval h based on initial conditions. h can be varied throughout the simulation at any point. The time step may be changed because the simulation has 'cooled' down significantly from the start, resulting in approximately stationary particles. It does not make sense to maintain the same step length irrespective of the particles average speed. A 'smart' step length was used towards the start of programming but later it was written out in favour of a fixed time step required for varying CCP.

SUB FUNCTIONS FOR THE CALCULATION OF GAMMA AND OTHER PARAMETERS

During most of the simulations very little data needs to be collected. Only during key stages, such as the addition of a particle or a significant change in CCP, should outputs be taken. Initially data was tabulated into columns. However, it became apparent for contour plotting that a 2-D array of 'z' points would be more suited. All data sets were then output in the new format allowing for easy integration into other data visualisation programs.

PCF CALCULATION

The PCF, known as G(r), is a measure of the average inter-particle separation. Each particle is taken in turn and the distance to every other particle measured and normalised based on the distance as r^{-2}. This results in a graph with successive peaks. The first peak is the shortest distance on average observed between particles i.e. twice the apparent radius of a particle (i.e. including charge effects). The following peaks show longer term structure throughout the crystal, including but not limited to successive shells and surface (shell) structure. Theoretically the PCF should tend to 1 at large R, but as the simulation is a finite system it tends to zero. The PCF is generally always scaled so that the highest peak = 1. This allows for easy data plotting.

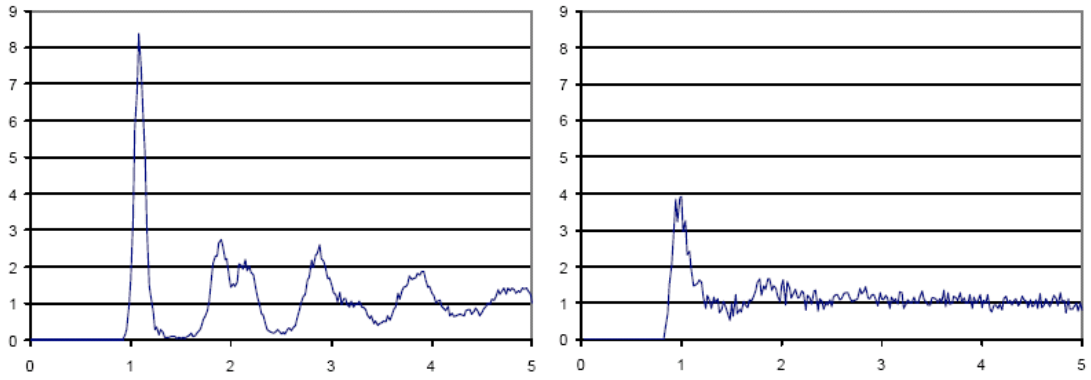

FIGURE 2: BOTH PCF'S ARE NORMALISED I.E. THEY TEND TOWARD 1 AS R(X AXIS) GROWS. G(R) IS ON THE Y AXIS. LEFT HAND SIDE IS SOLID CRYSTAL WHEREAS RIGHT HAND SIDE IS LIQUID CRYSTAL. NOTE THE LACK OF DISTINCTION BEYOND THE SECOND PEAK FOR THE LIQUID CRYSTAL (RIGHT HAND SIDE).

Using the PCF it is possible to easily differentiate between well ordered and unordered systems.

SHELL STRUCTURE

Many 2-D examples of this are shown throughout the report. It should be noted that the shell structure is the number of particles at R normalised by r^{-2}, analogous to areal density. The maximum 'density' value is also always scaled to 1. The shell structure is rescaled every time it is measured. This can lead to 'odd' results were number densities seem to fluctuate within a shell. This can occur if a rogue particle drifts towards the centre of the apparatus and is thus

normalised to 1 (due to the low R value). Then, all other values, through scaling, approach zero. The 'raw' data can be recovered from the data files and used to reconstruct the true value discarding the anomalous particle. The normalising factor is also always included in the data output.

POTENTIAL & E-FIELD

The E-Field was calculated by summing the charge of all the dust grains within a radius R and subtracting the average positive background charge enclosed within the volume at R (calculated by summing the charge on all the dust grains, flipping the sign, and then dividing by the volume of the apparatus). This value was then divided by the surface area swept out by a shell at R. If the 'wall' of the apparatus is removed within the program particles given sufficient energy can leave the apparatus leaving an overall positive charge. Through numerically integrating the E-Field the potential is obtained.

THE PHYSICS MODEL

CONSTANTS, VARIABLES AND NORMALISATION

For normalised units and how they were calculated see Appendix A. During the simulation only Newton's Laws of Motion, Coulomb electrostatic forces, gamma and temperature were routinely calculated by the program. All constants such as the charge of an electron and silicon's density (set as the dust density) were stored in global_vars.h.

Dust charge was based on a charge per unit radius, stipulated by the user at the start of each simulation – variable mass dust grains would all be scaled accordingly. The charge on a dust grain varies linearly with its radius (Orbit Motion Limited theory).

When all the variables in Appendix A are calculated at the start the simulation all the necessary information needed to model a dusty plasma has been generated.

BOUNDARY CONDITIONS

The only boundary condition required within the simulation is that the electric field goes to zero at the edge of the apparatus due to quasi neutrality. This is achieved by ensuring the background plasma charge density over the volume of the apparatus is equal to the total charge on all the dust particles. This also ensures that the electric field at the centre is 0 (no background charge at distance 0) and that the potential at the edge is 0 (no net charge thus no net potential).

It was assumed that the electric field increases linearly with distance from the centre of apparatus (while inside the sphere) then falls by r^{-2} outside the sphere. The force on a particle within the simulation was calculated by working out the attractive force from the E-Field (the background plasma) and then subtracting the 'repulsive' forces from the surrounding dust particles. This net force was used to calculate its acceleration, velocity and position.

VISUALISATION

Matlab and Excel were used to generate contour and scatter plots respectively. Due to the massive volume of data, the data was often decimated by a factor of 10 for ease of handling – Matlab struggles to plot over 100,000 data points and excel can only display 65k rows of data. As all the maxima of the outputs mentioned in the previous section are scaled to 1 in the 2-D outputs, the coloured contours in use by Matlab are consistent in all the filled and line 2-D contour graphs.

CONTROLLING THE SIMULATION

During the simulation it is necessary to control the CCP and hence the temperature of the particles. To achieve this an 'intelligent' cooling system was utilised. The cooling system would create a linear drag or acceleration force respectively decreasing or increasing the velocity by approximately 1% per time step interval. As the CCP continually fluctuates over time due to small disturbances within the crystal an 'accuracy' threshold of 1% is given to the control of the CCP. Once the desired temperature has been reached it is maintained through actively cooling and heating the simulation. Simply slowing down the particles does not create a well aligned crystal and the particles must be given time to move into their equilibrium positions. Thus turning the cooling system repeatedly on and off allows the dust particles to reach their most stable configuration. Once a CCP/temperature has reached its target (within a threshold tolerance) for 10 consecutive time steps, cooling becomes passive. Measurements of the CCP are only taken every 10 time steps rather than every time step (increases speed of simulation) and only if the 'average' value of the last 10 readings fluctuates from the target CCP by more than the threshold is 'active' cooling once again enabled. By repeating this process over long periods of time very stable crystal lattices can be created. At very high CCP (>2000) any small movement by just a few particles can lead to a large fluctuating CCP value. This must just be accepted as a by-product of the simulation.

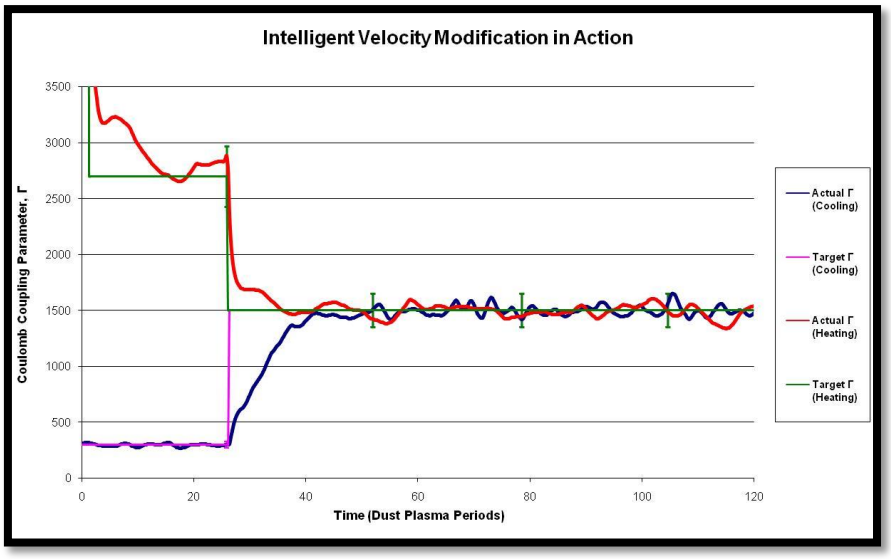

FIGURE 3 : SHOWING HOW THE 'INTELLIGENT' COOLING/HEATING SYSTEM REACHES A TARGET CCP VALUE AND MAINTAINS IT OVER A PERIOD OF TIME. THIS GRAPH WAS TAKEN FROM DAVID SHONE'S MSCI REPORT[12].

SHELLS

The simulation is started from an unordered random distribution of dust particles with a uniformly distributed background charge of equal but opposite charge. The electric field and potential at the start of the simulation are shown below:

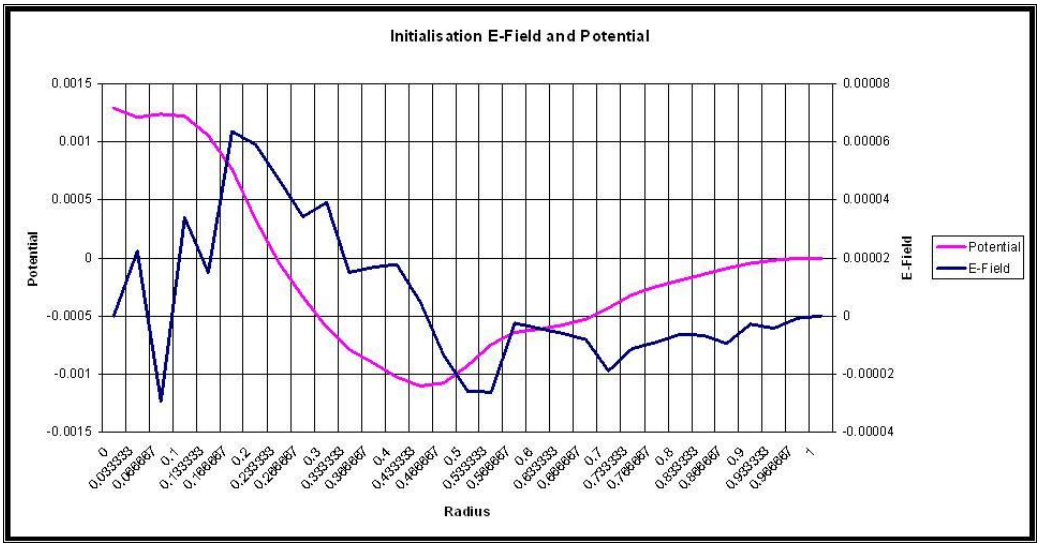

FIGURE 4: THE UNORDERED START POTENTIAL AND E-FIELD AS A FUNCTION OF UNIT RADIUS FROM THE CNTRE OF THE SIMULATION

As the dusty plasma is cooled shell formation occurs. For shell structure see page 13, for shell growth see page 9. As this occurs the electric field stabilises from initialisation to a roughly uniform pattern, as does the potential. Below is Figure 5 showing the E-Field and Potential of 655 particles at a CCP of 300.

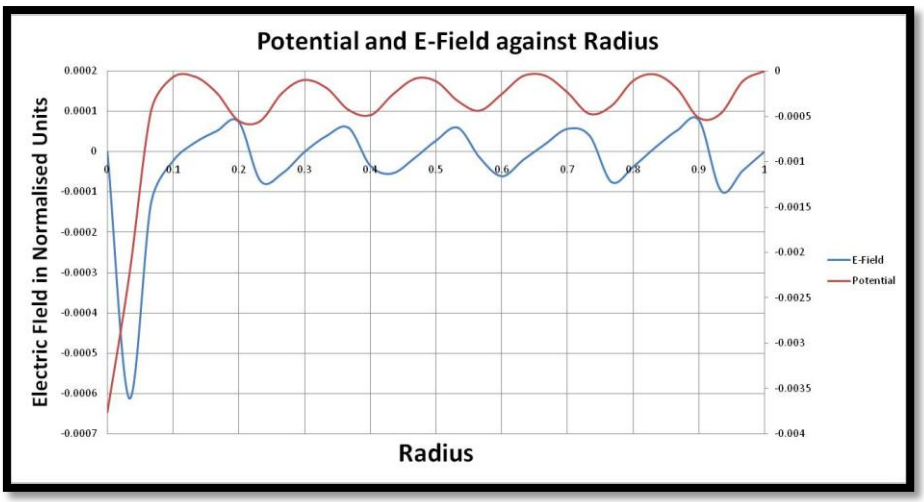

FIGURE 5 : SHOWING HOW POTENTIAL AND E-FIELD VARY ACROSS CRYSTALLISED DUSTY PLASMAS. THE MINIMA OF POTENTIAL CORRESPOND TO AREAS OF HIGH PARTICLE AREAL DENSITY (I.E POINT AT WHICH SHELLS LIE). THE ELECTRIC FIELD ON AVERAGE IS 0 (THE POTENTIAL TENDS TO 0 AS R TENDS TO 1). THE LEFT HAND AXIS IS FOR THE E-FIELD (BLUE) WHEREAS THE POTENTIAL (RED) IS ON THE RIGHT HAND AXIS.

Due to normalisation effects as R→0 as well as numerical instabilities at R=0 the graphs veer 'off course' at low R values. Towards the centre there are no particles, so only the positive background remains, until about 0.05 radii outwards where the first particles occur. This can be seen as a change from negative to positive gradient in the electric field. The E-Field's total flux is minimal as the surface area over which it is measured is proportionately small. As soon as a particle attempts to 'enter' this region the average charge flips 'sign' (this occurs at the point where the particle is) due to the charge on the dust grain. As it approaches the centre the force inwards becomes ever less, but now there is a 'positive' shell left outside of the particle. Thus it drifts back to its original location.

However, the general trend further out is far clearer. A sinusoidal E-Field (hence Potential) forms stable points were shells are located. This is the most energetically favourable arrangement because the forces have been minimised and charge neutrality has been conserved over most of R to a very high degree. Below on the same x axis are the shell areal densities (left hand axis) plotted with the potential as above.

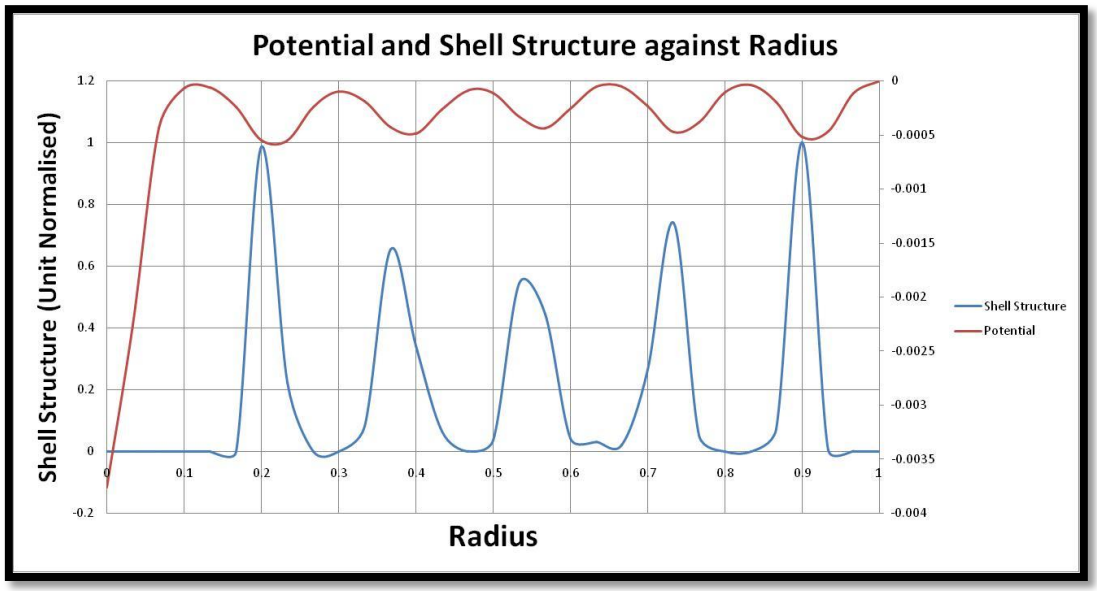

FIGURE 6 : NOTE HOW MINIMA IN THE POTENTIAL CLEARLY COINCIDE WITH PEAKS IN THE UNIT NORMALISED SHELL STRUCTURE AS EXPECTED. THIS IS THE MOST ENERGETICALLY FAVOURABLE STATE FOR THE CRYSTAL SHELL STRUCTURE TO BE ARRANGED. MOST OF THE PARTICLES ARE LOCATED TOWARDS THE EDGE OF THE APPARATUS BUT DUE TO NORMALISATION THE INNER MOST PEAK HAS BEEN NORMALISED TO APPROXIMATELY 1 (REDUCING THE APPARENT HEIGHT OF THE MIDDLE PEAKS)

This type of arrangement can be seen for any number of particles. With higher numbers of particles the number of shells increases as does the corresponding number of minima in the potential.

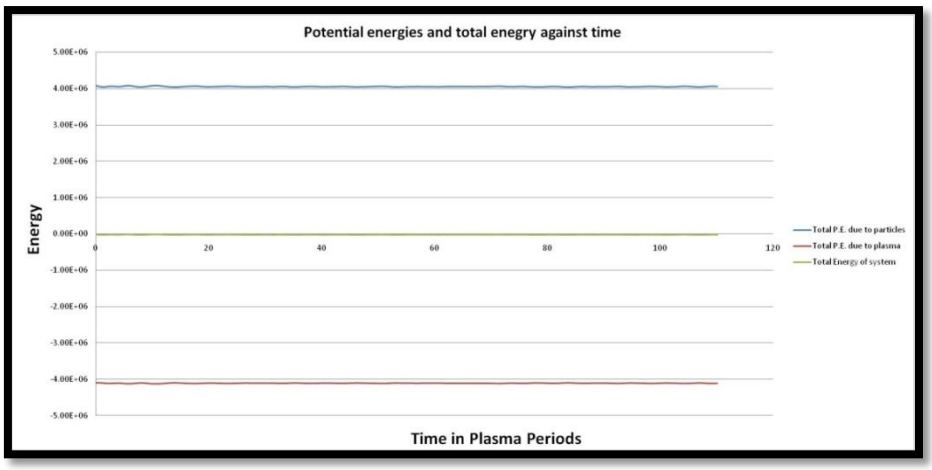

FIGURE 7 : SHOWING THE POTENTIAL ENERGY BETWEEN ALL THE PARTICLES COULOMB REPULSION (BLUE) AND THE POTENTIAL DUE TO THE BACKGROUND CHARGE (ATTRACTIVE TO ALL THE PARTICLES AND IN RED). THE OVERALL ENERGY OF THE SYSTEM (GREEN) IS JUST NEGATIVE IN RELATION TO THE POTENTIAL ENERGIES.

The potential energy of the plasma almost perfectly balances out that due to the repulsion of the particles. At a high enough CCP (generally above 1) it is possible for liquid/solid crystal lattices to form.

SHELL GROWTH

By repeatedly adding particles into the simulation, allowing the apparatus to expand naturally (i.e. keeping the average inter-particle distances the same, as calculated at the start of the simulation) and cooling the particles down after the addition of a new particle, shell formation was observed. Upon the addition of a new particle kinetic energy is imparted to the system. This must be removed otherwise over time the system would slowly become unstable. The 'intelligent' cooling mechanism mentioned under 'Controlling the Simulation' controls the overall ratio of kinetic energy to potential energy of the system so that it remains constant.

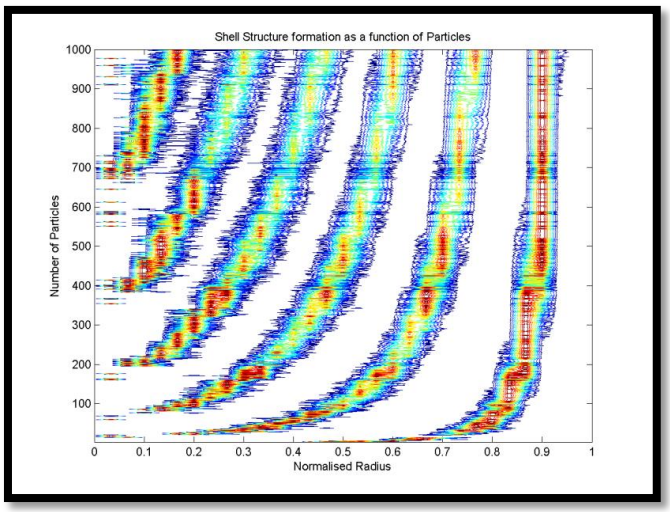

FIGURE 8: FORMATION OF SHELLS. AS THE NUMBER OF PARTICLES INCREASES THE NUMBER OF SHELLS ALSO INCREASES. IT SHOULD BE NOTED THAT THE NORMALISED RADIUS IS 'RE-NORMALISED' FOR EVERY POINT ON THE GRAPH. THUS 0.9 RADIANS DOES NOT CORRESPOND TO A FIXED ABSOLUTE DISTANCE. AS MORE PARTICLES ARE ADDED TO THE SIMULATION THE TRUE RADIUS IS INCREASING AS SHOWN IN FIGURE 9 ON PAGE 10 BELOW.

Particles were always added from the centre of the apparatus while conserving charge neutrality within the simulation. Although the phase change CCP value is theoretically predicted at 172 a slightly higher value of 300 was chosen for the cooling target at which data would be read out from the simulation, and thereafter a new particle added into the system. This was to ensure that a crystal had formed before the shell structure and PCF were analysed.

The above graph clearly demonstrates shell structure formation. As the number of particles is increased (ascending y) the number of peaks seen in the unit normalised particle numbers along the radius apparatus increases. For every consecutive shell to be formed an exponential increase in the number of particles is required in relation to the previous shell. To determine the shell structure type an accurate gauge of particle numbers within each shell will have to be made as well as a study into the specific numbers required for the formation of a new shell. Through casual observation of the crystals it can be determined that the surface structure is almost entirely hexagonal with little variation.

From Figure 9 below the relationship between radius and the number of particles can be clearly seen. The graph follows a power law relation:

$$y = 2 \times 10^{-5} x^3$$

EQUATION 4 : RELATION BETWEEN PARTICLES (Y) AND RADIUS (X)

The r squared fit value for the above equation is 1.00 ± 0.005.

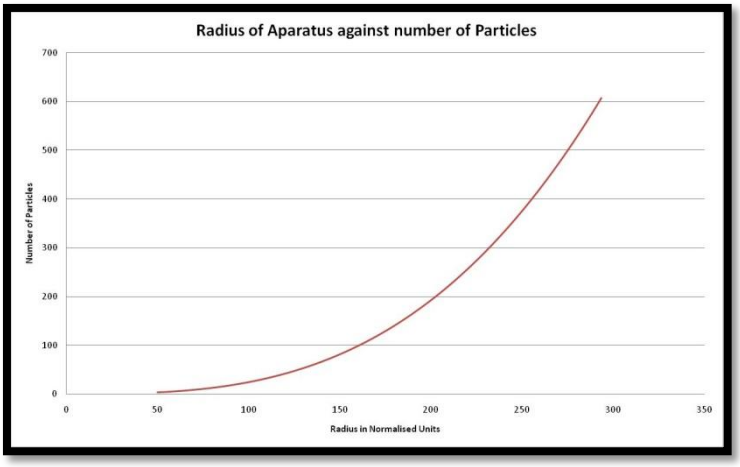

FIGURE 9: SHOWING HOW RADIUS VARIES WITH THE NUMBER OF PARTICLES WITHIN IT AT A FIXED INTER-PARTICLE DISTANCE.

This shows how the apparatus is expanded to accommodate the addition of new particles while keeping the average particle number density equal (hence the cubed relation).

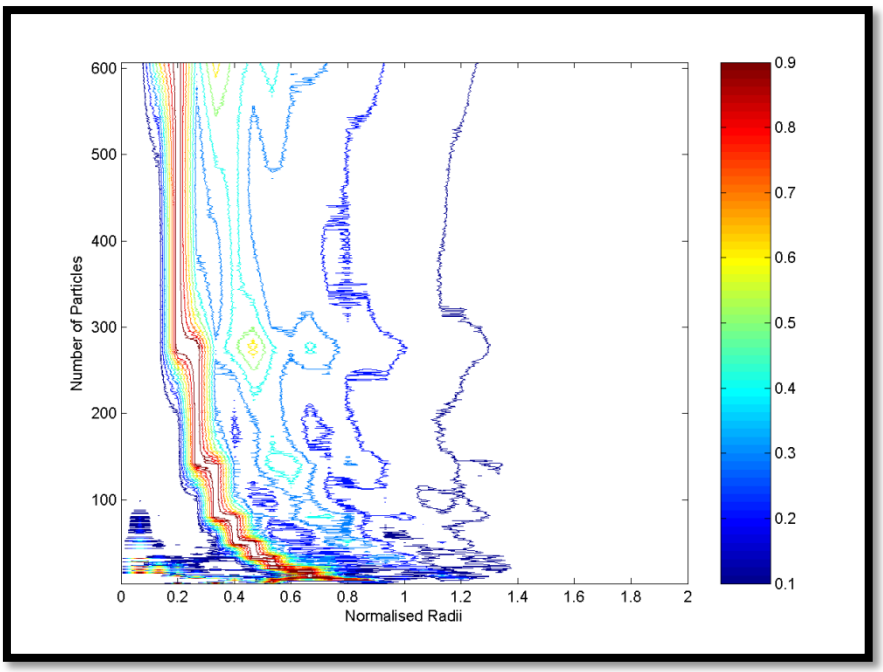

FIGURE 10: A CONTOUR PLOT OF HOW THE PAIR CORRELATION FUNCTION (PCF) VARIES WITH RESPECT TO THE NUMBER OF PARTICLES. NOTE THE AREAS OF SUDDEN SHIFTS WITHIN THE PCF (FOR INSTANCE JUST BELOW 300 PARTICLES) SHOW WHERE SHELL STABILITY HAS BEEN MAXIMISED. THIS CAN ALSO BE SEEN BY THE FORMATION OF VERY CLEAR SECONDARY AND TERTIARY "PEAKS" ON THE PCF. THESE ARE INDICATED BY THE CONTOURS AT VARYING RADII.

The shifts in PCF do not correspond to new shell formation points. Instead these occur just before the formation of a new shell. As particles are added to the crystal there will not be enough particles to 'fill' all the shells so the 'average' separation between particles will appear larger than it should do on the PCF. Once a critical number has been reached there is a sudden increase in system stability seen as a shift in PCF, this occurs when all the shells are filled and the crystal structure has no 'imperfections' or 'missing' particles (decreased average distance between particles). This is analogous to atomic shell orbitals. There is an increase in order signified by the secondary and tertiary peaks in the PCF. Then more particles are added which over fill the shell. During this time the system is expanding, hence the shells themselves increase in size to accommodate the new particles, which is why there is not an immediate shift back to the previous unstable configuration PCF value when too many particles are added. Soon thereafter a new shell is formed in which new particles will be added until the system is once again stable.

These areas of increased stability occur at the following particle numbers:

20±1 34±2 51±2 81±3 142±3 276±4 655±5

If an exponential of the form $number\ of\ particles = Ae^{B^{Stable\ Point}}$ is fitted to the data (with an r squared value of 0.999±0.0005) the next value was estimated to lie at 2137±7 particles. Numerically solving this gives A=16.62 and B=1.29. Due to the length of the process (53 hours of computation time was required to create the above plot) this value had to be identified by sweeping the range 2050 – 2090 particles.

To check these values the same simulation was run again but this time the particles had a charge of 7000e.

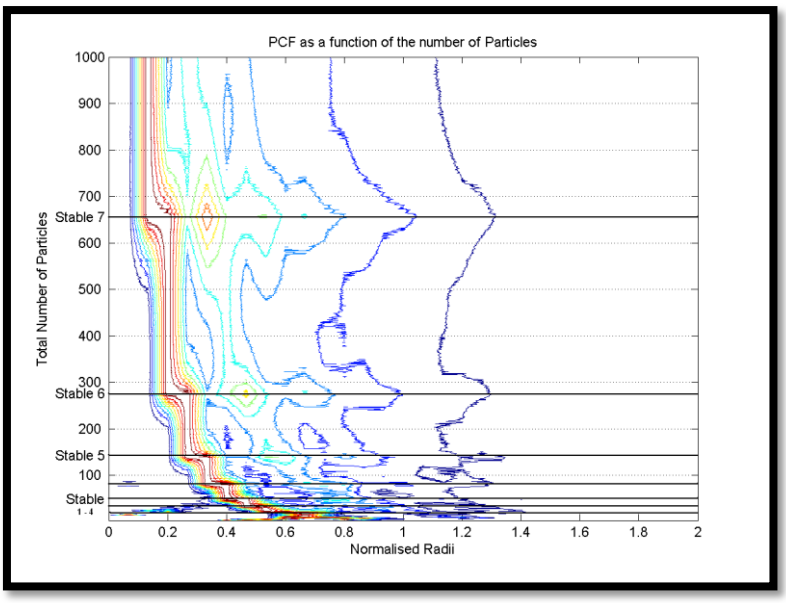

FIGURE 11 : A CONTOUR PLOT OF HOW THE PAIR CORRELATION FUNCTION (PCF) VARIED WITH RESPECT TO THE NUMBER OF PARTICLES. SAME AS FIGURE 10 EXCEPT THE PARTICLE CHARGES HAVE BEEN REDUCED BY 30% TO 7000 ELECTRON CHARGES. NOTE THE SYSTEM BEHAVES IDENTICALLY AS BEFORE.

In Figure 12 on page 12 below, the 8th stable point can be just made out as a shift in the maximum peak towards the left of the figure. It is evident the exponential relationship between stable point and total number of particles seems to hold. A higher resolution cross section at 2130 particles can be seen in Figure 13 on page 13.

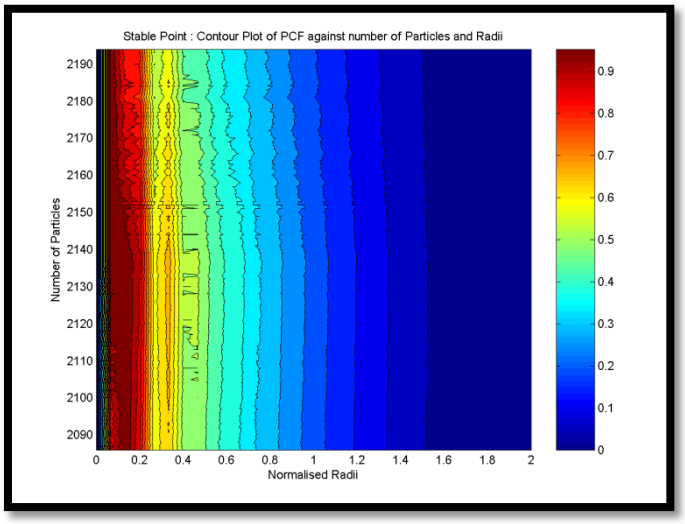

FIGURE 12 : SHOWING THE 'NEXT' STABLE POINT FOUND AT 2130 PARTICLES. THE REASON LONG TERM STRUCTURE IS NO LONGER VERY EVIDENT IS DUE TO THE RESOLUTION BEING TOO LOW (THERE ARE ONLY 30 SAMPLES ALONG THE X AXIS). SEE THE NEXT FIGURE FOR A HIGH RESOLUTION CROSS SECTION OF 2130 PARTICLES.

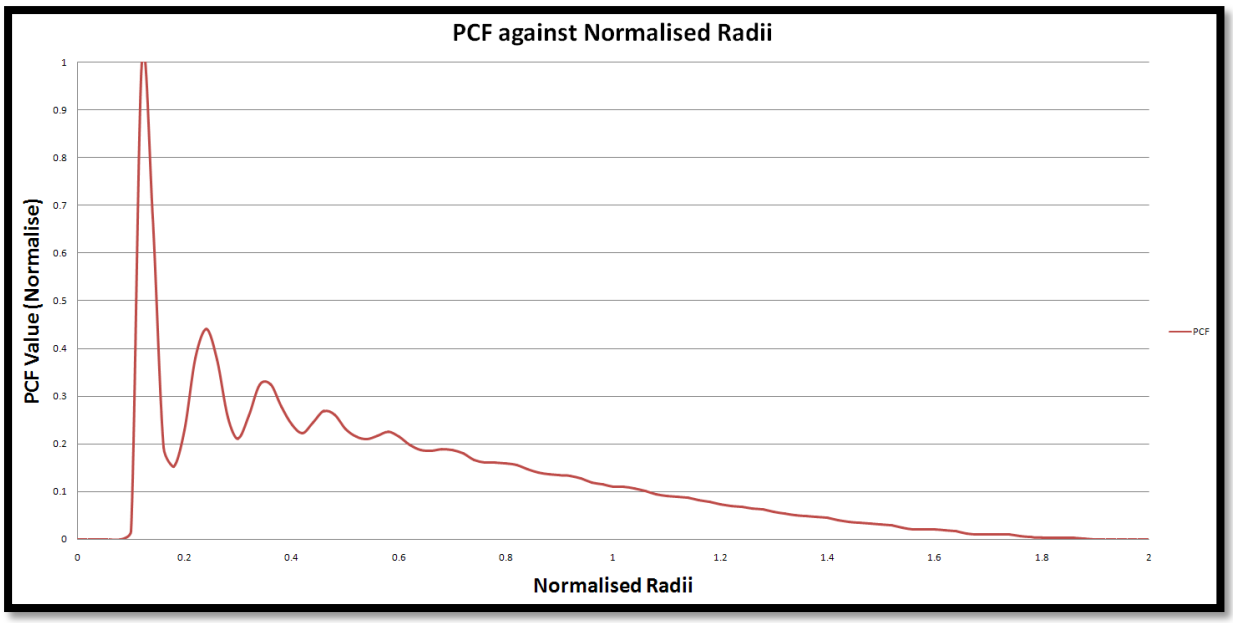

FIGURE 13 : SHOWING A HIGH RESOLUTION (100 'X' SAMPLES) PCF OF 2130 PARTICLES AT 500 CCP. IN COMPARISON TO FIGURE 12 ABOVE THERE IS CLEARLY A LOT OF LONG TERM STRUCTURE EVEN UP TO 0.6 RADII AWAY.

CRYSTAL STRUCTURE

Due to the spherical nature of the apparatus the crystal may well be biased towards a spherical geometry, but through increasing the number of particles edge effects should dissipate from the inner shells, leaving the 'natural' structure behind. Below, on page 13, are Picture 1, Picture 2 and Picture 3, graphically demonstrating the proposed hexagonal close packed nature of the crystal.

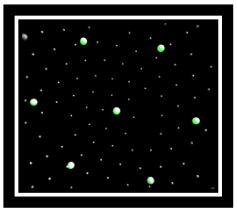

PICTURE 1: SCREEN CAPTURE OF THE PROGRAM SHOWING THE HEXAGONAL STRUCTURE OF THE LATTICE WITHIN ONE SHELL.

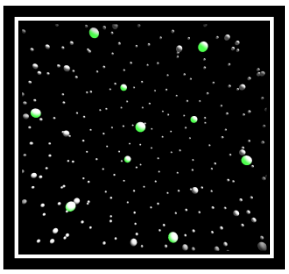

PICTURE 2: THE SAME PARTICLES AS THOSE IN PICTURE 1 ABOVE, BUT THIS FIGURE ALSO SHOWS THE LAYER BELOW. COMPARE TO PICTURE 3 BELOW.

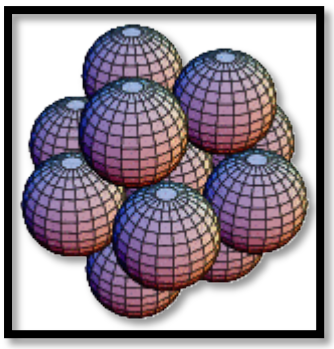

PICTURE 3: A GRAPHICAL REPRESENTATION OF HEXAGONALLY CLOSE PACKED PARTICLES [13]. CLEARLY A HEXAGONALLY PACKED STRUCTURE WOULD APPEAR TO BE PRESENT (VISUALLY) IN PICTURE 2.

From experimental observations [14] it has been determined that dusty plasmas form hexagonally close packed lattices. If the 'spheres' within this structure are allowed to expand uniformly until the 'spheres' fill all the gaps, an irregular dodecahedron consisting of 6 rhombi and 6 trapezoids will be formed [13].

If it is assumed that the particles are hexagonally close packed then the unit cell count is 3. Taking this value, the stable particle conditions can be adjusted to give possible values within one standard deviation as follows:

21	33,36	51	78,81,84	139,142,145	273,276,279	651,654,657,660	2124,2127,2130,2133,2136

TABLE 1 : SHOWING THE POSSIBLE NUMBERS OF PARTICLES REQUIRED TO CREATE THE FIRST 8 'STABLE' POINTS. GIVEN THE UNIT CELL COUNT OF 3, ALL THE VALUES MUST BE DIVISIBLE BY 3.

Using the stable points found in '

Shell Growth' a study of the final four points yields the following table:

Particles	HCP	Error	SC	BCC
142	96%	5%	108%	99%
276	96%	6%	107%	98%
654	96%	8%	108%	99%
2130	95%	12%	106%	98%

TABLE 2 : SHOWING WHAT FRACTION OF THE ACTUAL RADIUS (AS CALCULATED BY THE PROGRAM) A GIVEN NUMBER OF PARTICLES WOULD NEED TO FIT INTO, IN ORDER TO BE HEXAGONALLY CLOSE PACKED. THE APPARENT SIZE OF THE PARTICLES WAS TAKEN TO BE ½ THE INTER-PARTICLE DISTANCE, WHICH WAS OBTAINED FROM THE FIRST PEAK OF THE CORRESPONDING PCF. THE FINAL TWO COLUMNS SHOW THE SAME VALUES FOR SIMPLE CUBIC AND BODY CENTRED CUBIC.

Simple cubic therefore cannot fit into the actual size of the apparatus given the inter-particle distance observed through the PCF. Hence only HCP and BCC remain. Although these could both physically fit within the sphere there are two points to consider.

1. BCC is visually very different to HCP which, as explained below is not seen within the simulation.
2. The volume efficiency factor is a maximum theoretical amount never actually observed in real life. So although BCC would fit within the apparatus, it is a very close fit and has comparatively very little room for error.

The only other common crystal structure type found is face centred cubic which has the same volume density as hexagonally close packed. Below is a diagram showing the crystal arrangement for a FCC crystal. By combining the results from Table 2, the visual observations (Page 13, Picture 1) and also Picture 4 below, the crystal structure of the numerical simulation can be regarded as hexagonally close packed.

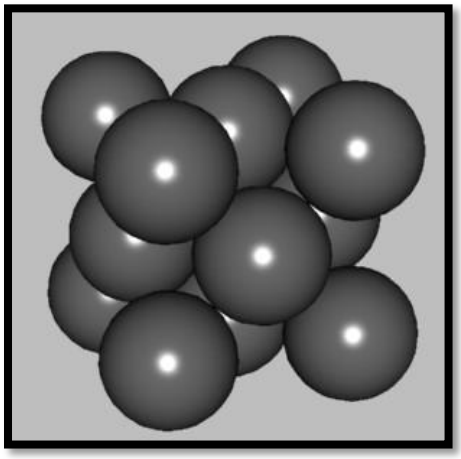

PICTURE 4 : THIS IS A DIAGRAM OF FACE CENTRED CUBIC (FCC) AND HAS THE SAME VOLUME DENSITY AS HEXAGONALLY CLOSE PACKED, BUT IS VISUALLY VERY DIFFERENT AND THUS CAN BE DISCOUNTED AS A POSSIBLE STRUCTURE TYPE.

Understanding how stable points occur will be very important in identifying the underlying physical principles in dusty plasma crystal formation. Within each spherical surface of the crystal the charged dust grains align themselves as shown in the following picture:

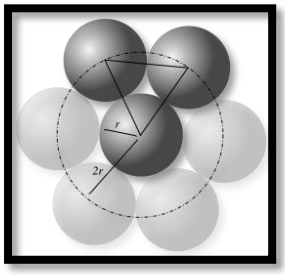

PICTURE 5 [15] : SHOWING THE SURFACE ARRANGEMENT OF A HEXAGONALLY CLOSE PACKED CRYSTAL

From [15] the surface density of the arrangement is 0.9069 or $\frac{\pi}{\sqrt{12}}$, which shall be denoted as ξ or 'packing efficiency'. For a stable crystal to form several criteria must be met:

1. Each shell must be a near perfect distribution of these hexagonally close packed surface crystals.
2. All the particles must be held within shells which are evenly spread throughout the crystal to maintain the lowest potential as well as charge neutrality.
3. The CCP must be at least greater than 172. Based on the simulation behaviour a value of around 220 should suffice. (This can be assumed true for calculation purposes)

HEXAGONAL DISTRIBUTION

The apparent radius of the dust particle plasma sphere (½ the average inter-particle distance as reported by the PCF) will be denoted as R_d and the radius of the apparatus, R_a. Any value

between 0 and R_a will simply by denoted as R. R_d for any of the investigated simulation parameters is the same value when measured at successive stable points.

If $R_d << R$ it can be assumed that the R_d would appear to take up an area of πR_d^2 , whereas the total area of a particular shell is $4\pi R^2$. Thus the following equation is derived where ξ is the packing efficiency:

$$\frac{4\pi R^2 \xi}{\pi {R_d}^2} = Number\ of\ Particles\ at\ R = N$$

$$R_d = R\sqrt{\frac{4\xi}{N}}\ so\ R_s \propto R\sqrt{\frac{1}{N}}$$

EQUATION 5 : THE RELATIONSHIP BETWEEN R_D (KNOWN THROUGH THE PCF) AND R RADIUS OF SHELL.

The surface unit cell count is 3 (1 in the middle and 6 more each shared with 3 cells). So N must be divisible by three at a particular R in order for a perfect shell. This must be computationally calculated. It is apparent that if an accuracy threshold is set (i.e. as the solution cannot be found analytically, a numerical accuracy parameter must be chosen), then the following graph can be produced:

$\left|\frac{N}{3} - ROUND\left(\frac{N}{3}\right)\right| < 0.01$; 0.01 x 3 = 0.03 Particles away from a perfect fit

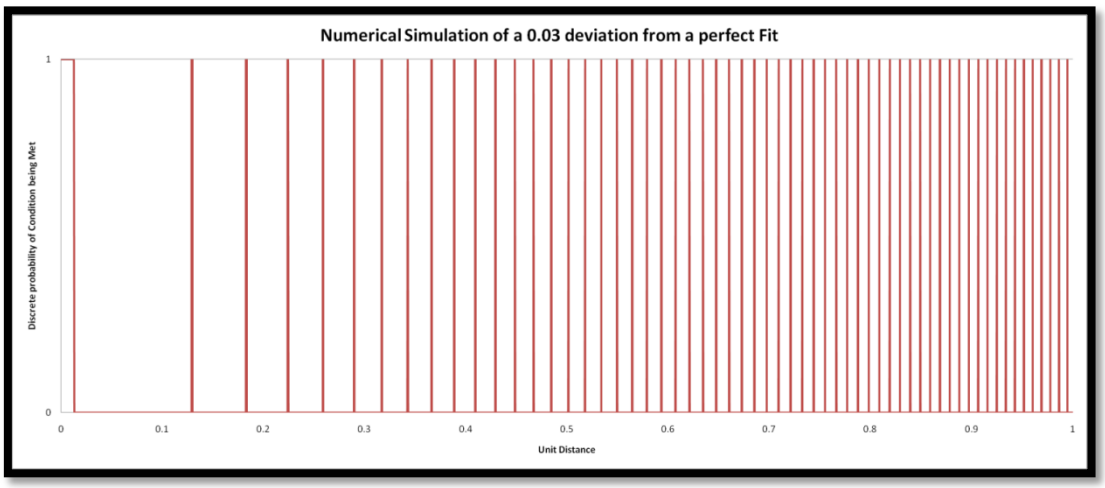

FIGURE 14 : SHOWING THAT AS THE DISTANCE INCREASES SO DOES THE OCCURRENCE OF 'NEAR-PERFECT' HEXAGONALLY CLOSE PACKED SURFACES. THIS MEANS THAT SHELLS FURTHER FROM THE CENTRE OF THE APPARATUS ARE MORE LIKELY TO BE STABLE AS ONLY A SMALL CHANGE IN R WILL ALLOW THE CRYSTAL SHELLS TO ALIGN THEMSELVES TO AN ALMOST PERFECT HCP SURFACE.

At each stable point the difference between R_d obtained through the PCF and R_d measured through the direct number of particles at R (c.f. Equation 5) is recorded. This is then weighted by the number of particles at R and further normalised by a factor of $\frac{1}{R^2}$ to get the following contour plot below:

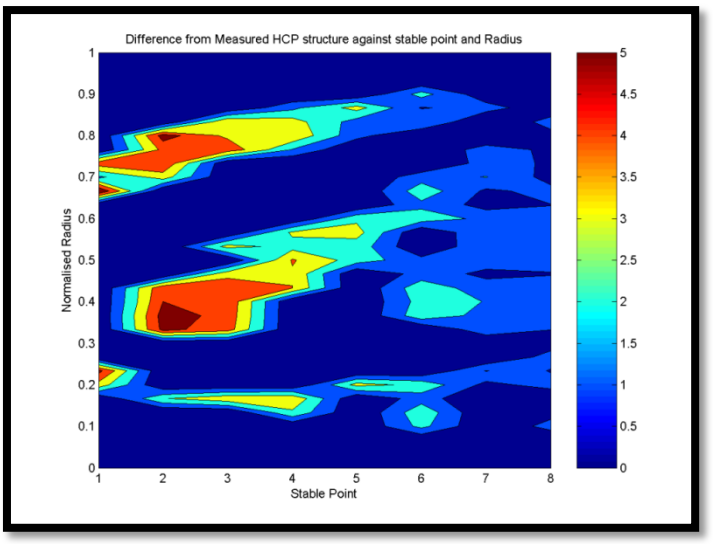

FIGURE 15 : A FILLED CONTOUR PLOT SHOWING THE MEASURED DIFFERENCE BETWEEN EXPECTED HCP SHELL CONFIGURATIONS AND MEASURED SHELL CONFIGURATIONS. NOTE THE INCREASED STABILITY AS HIGHER STABLE POINT NUMBERS ARE REACHED.

Figure 15 above demonstrates how the simulation creates almost perfect surface shell crystals (especially at higher Stable Points). This can be explained because the radius is increasing (due to the number of particles increasing), as shown in Equation 4 and Figure 9 on page 10, so the number of "possible" stable points (where a perfect HCP surface would be observed) is also increasing with distance from the centre of the apparatus as shown in Figure 14. This allows for better long and short term structure because of the increased order within the crystal. This can be seen through many successive peaks within the PCF in Figure 13 on page 13.

The following table results were calculated by measuring the inter-particle separation and working out the volume and surface packing efficiencies:

Particles	142	276	655	2129	
Surface Packing Efficiency	86%	90%	90%	88%	**Average 89%**
Standard Deviation	6%	2%	9%	5%	**Average 6%**
Volume Packing Efficiency	66%	65%	66%	63%	**Average 65%+/-1.2%**

TABLE 3: SHOWING HOW SURFACE PACKING DENSITIES AGREE CLOSELY WITH EXPECTED HCP EFFICIENCY (90%). HOWEVER, VOLUME PACKING EFFICIENCY DIFFERS BY 9% (EXPECTED 74%)

During high N simulations very similar results were achieved for the outer most shells. However, towards the centre of the apparatus much more widely varying densities were seen. See "High Particle Number Simulations" on page 22 for more details.

SHELL SEPARATION

In order to 'analytically' derive an expression for the number or particles required for a 'stable' point two more factors must be taken into consideration. It may need to be found numerically, however this is far less intensive than running the dusty plasma simulation.

1. With every successive particle added the apparatus expands, as do the shells. This increases the number of particles they can hold.
2. Shells appear to be evenly distribution across R but if there is a small deviation from this even distribution compounded errors could result in a large mismatch between estimated particle numbers and measured particle numbers.

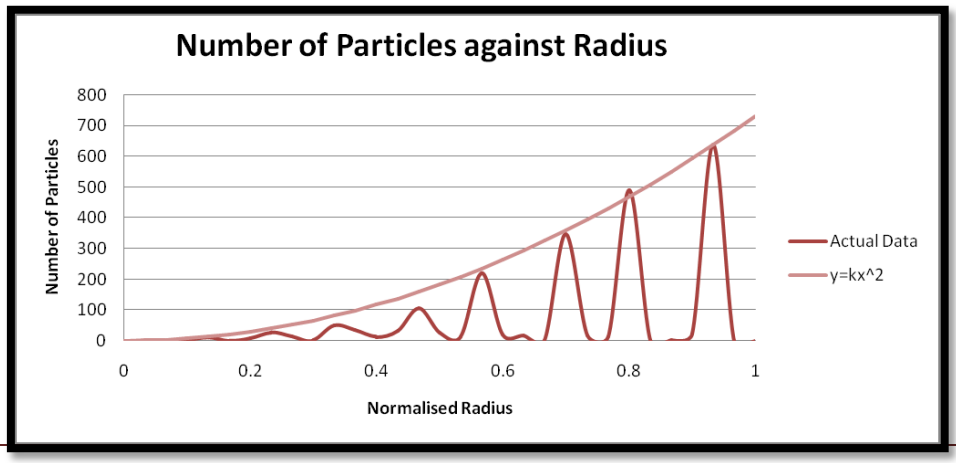

FIGURE 16 : THE ABSOLUTE NUMBER OF PARTICLES VARIES AS $N=KR^2$, WHICH IS IN LINE WITH THE EARLIER PREDICTION. THIS DISTRIBUTION WAS ALSO SEEN IN [16].

Figure 16 demonstrates the discrete shell structure for 2130 particles (the 8th stable point). On average the shells are evenly distributed.

In hexagonally close packed lattices the separation between one layer and the next is $\sqrt{\frac{2}{3}}R_d \times 2$ [17]. If the shell formation graph is taken and marked at the expected points where new shells should form, there is a clear discrepancy as R decreases (c.f. Figure 8). The outer shell is constrained by the edge of the apparatus. Thus it must be approximately R_d away, as otherwise the particles apparent size would be outside the apparatus. However, the outer shell is most affected by edge effects. On the outer shell we see clear evidence of hexagonal surface structure. Further within the apparatus the particles form a different shell structure, which although close to hexagonal surface structure is different when viewed in 3 dimensions (it has the surface structure but the layers are not aligned correctly).

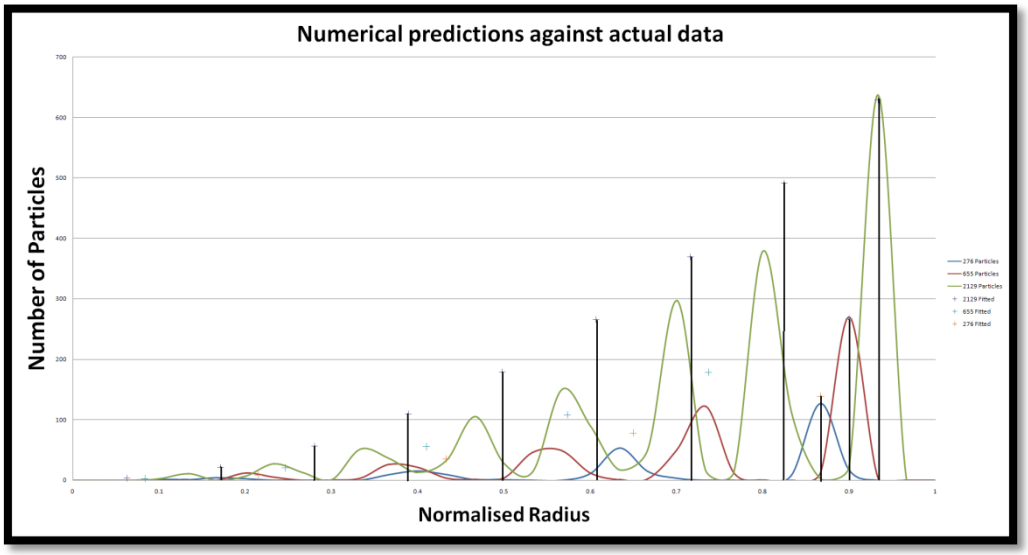

FIGURE 17 : NOTE THE DRIFT AWAY FROM WHAT IS EXPECTED IN HCP LAYER SEPARATION. THIS IS DUE TO A DISCREPANCY IN THE SHELL SEPARATION, LEADING TO A COMPOUND ERROR WHICH LEADS TO AN UNACCEPTABLY HIGH ERROR TOWARDS THE CENTRE OF THE APPARATUS. THE BLACK VERTICAL LINES SHOW THE EXPECTED NUMBER OF PARTICLES AT THE EXPECTED SHELL POISTIONS (GIVEN HCP SHELL SPERATION). NOTE HOW THIS MATCHES THE FIRST THREE PEAKS (2129, 655 AND 276 PARTICLES) VERY WELL BUT DEVIATES FURTHER FROM THE EDGE.

From this it can be deduced that the layers are hexagonally packed, but the separation between the layers is inconsistent with hexagonally close packed possibly due to edge effects.

NUMERICAL SOLUTION TO THE STABLE SHELL PROBLEM

Using all the above criteria the equations below attempt to solve the stable shell problem:

$$\sum_{i=S_1}^{S_n} \frac{4{R_i}^2\xi}{{R_d}^2} = N \; where \; R_i = Radius \; at \; shell \; 'i' and \; S_n = Shell \; number \; n$$

EQUATION 6 : THE RELATIONSHIP BETWEEN N AND HOW MANY SHELLS THERE ARE.

$$Condition: \left|\frac{4{R_i}^2\xi}{3{R_d}^2} - ROUND\left(\frac{4{R_i}^2\xi}{3{R_d}^2}\right)\right| < threshold \in i$$

EQUATION 7 : CONDITION FOR ALL SHELLS TO BE 'NEAR-PERFECT' HCP STRUCTURE.

$$R_1 = R_a - R_d \; and \; R_i(for \; i > 1) = R_{i-1} - 2\sqrt{\frac{2}{3}}R_d$$

EQUATION 8 : THE POINTS AT WHICH THE ITH SHELL WILL OCCUR.

A numerical process could operate by asking how many shells (n) (i.e. stable point number) it should look for. Then it would calculate at what R_a ratios this would occur (c.f. Equation 8). It would then increase R_a and for each R_a check the HCP condition for all *i=0* → *i=n* from Equation 8. If the condition was satisfied then N would be calculated from Equation 6.

COULOMB COUPLING PARAMETER

If the CCP value drops below 172 a crystal should no longer be able to form [1]. Thus within the simulation a crystal was formed and the CCP slowly varied.

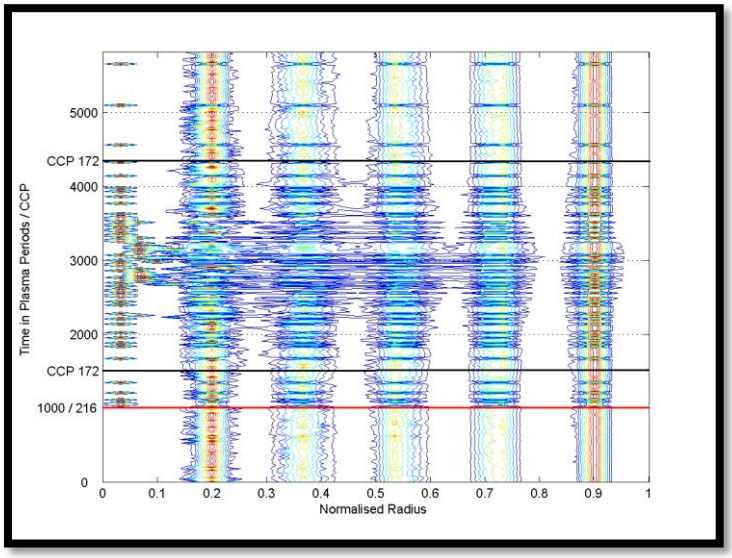

FIGURE 18: SHOWING THE VARIATION OF THE SHELL STRUCTURE AS CCP IS VARIED FOR 620 PARTICLES. NOTE THE CLEARLY FLUID PHASE BETWEEN CCP 172

In this rendering a crystal of 620 particles was taken from a CCP of 300 – 100 – 300 (bottom to top). It can clearly be seen that there is a distinct phase change between the CCP 172 regions (marked by the black horizontal lines). However, it is not entirely clear at what point the phase change actually starts. Also shown in Figure 18 above is the CCP line of 216, which seems to be the transition point. It becomes very difficult to differentiate between a solid and liquid close to the region's boundaries, as not all parts of the crystal may start to 'melt' at the same time. Lower particle numbers have less defined 'melt' points. This can clearly be seen in Figure 19, below on page 20.

A further feature of these graphs is the stability of the outer shell in comparison to the inner shells. This could be due to one or both of the following reasons:

1. Edge effects of the simulation create an artificially stable outer shell due to confinement in r (spherical polar co-ordinates).
2. The outer shell contains the largest number or particles and so has stability most resistant to small fluctuations. This could be viewed as an inherent stability.

With reference to point 2, typical shell configurations in absolute (un-normalised) particle numbers may be 8, 35, 81, 152, thus over half of all the particles are contained in the outer shell. This fraction varies with the number of particles as shown in Figure 20 on page 21.

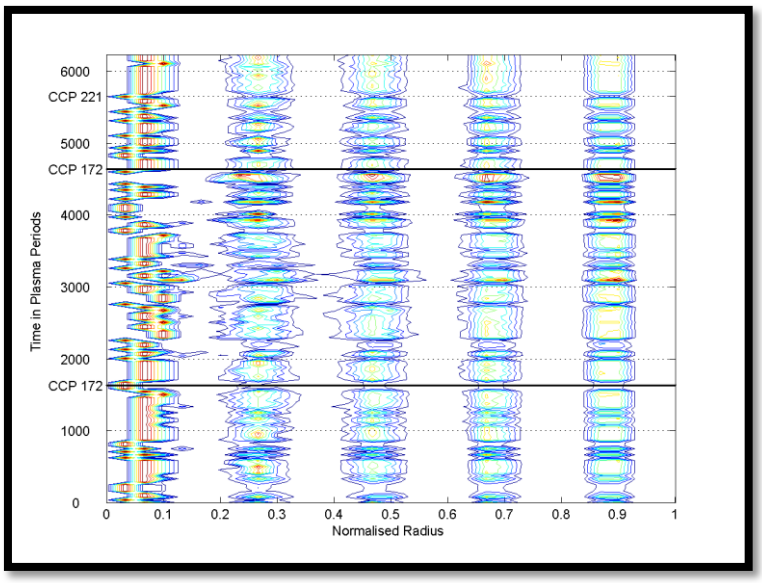

FIGURE 19 : ONLY 200 PARTICLES WERE USED IN THIS SIMULATION. IT IS CLEAR THAT THE BOUNDARY POINTS ARE NO LONGER WELL DEFINED AS THOSE IN FIGURE 18 ABOVE ON PAGE 19.

The following plot shows how the number of particles in the outer shell varies at increasing stability points, note the apparent logarithmic trend:

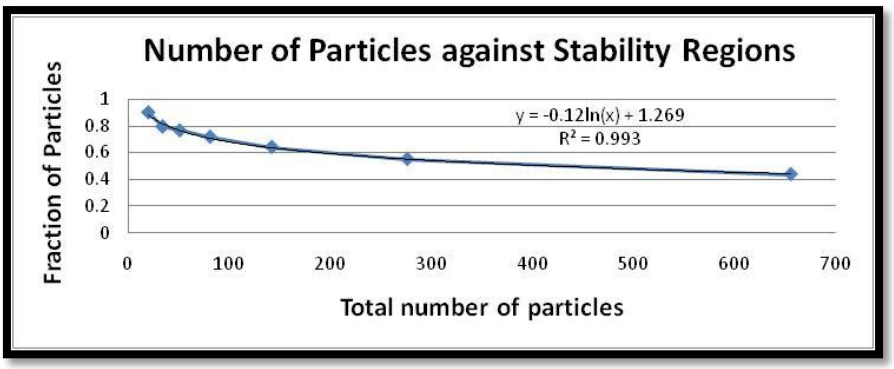

FIGURE 20 : SHOWING HOW THERE IS A LOGARITHMIC DECREASE IN THE FRACTION OF PARTICLES HELD IN THE OUTER SHELL IN CONSECUTIVE STABILITY POINTS. THUS AS N, THE NUMBER OF PARTICLES IS INCREASED THE SIMULATION SHOULD SLOWLY BECOME EVER LESS AFFECTED BY EDGE EFFECTS. HOWEVER, SIMULATION TIMES VARY WITH ORDER N^2 SO THERE IS A TRADE OFF BETWEEN ACCURACY AND SPEED.

Many previous simulations [18] have simulated a 2-D lattice. The advantage is edge effects can be observed at relatively low particle numbers (approx. 400 particles). However, within a 3-D structure it would require some 8000 particles to witness these edge effects clearly. To simulate 20 times more particles would require 200 times longer than the 400 particle simulation. This consequence of 3-D simulations may explain the apparent shift between expected and actual results commented in Figure 17 on page 18 under 'Shell Separation'.

VARYING CHARGE AND MASS

Within the simulation there is the option of having multiple mass, charge and radius dust particles. If multiple masses are used they are evenly distributed around the simulation at initialisation, as with only single mass simulation conditions. Below is a plot of particle distribution throughout the sphere at a CCP of 400, 656 particles and using 4 different mass's whose radii are 4,3,2 and 1 times that of those used in the previous simulations. There are 159 particles of each mass/radii/charge type.

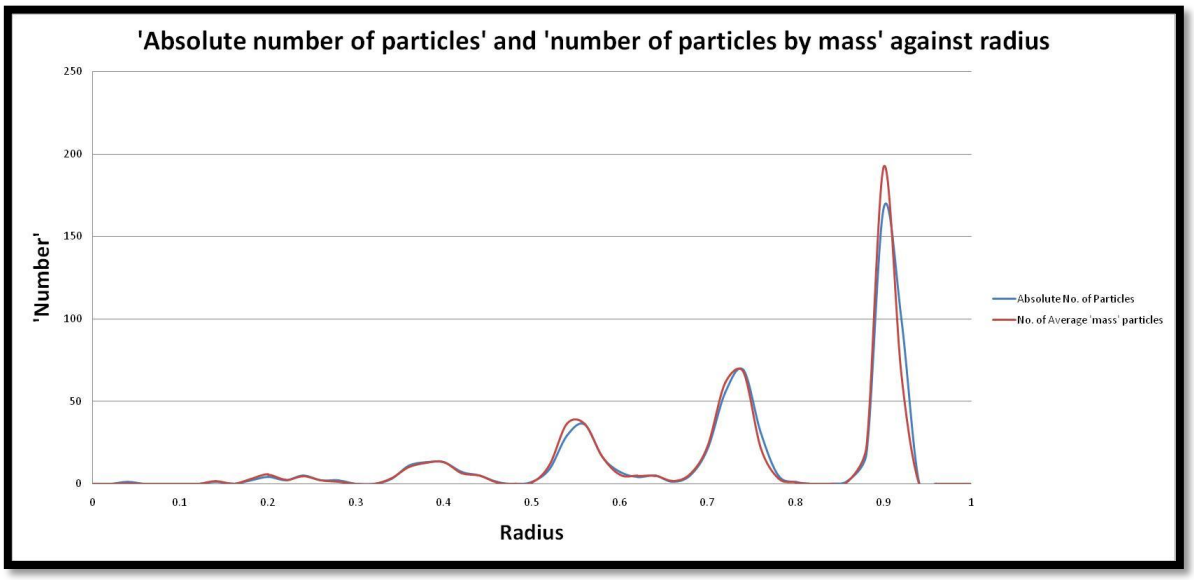

FIGURE 21 : SHOWING HOW THE PARTICLES ARRANGE THEMSELVES EVENLY ACROSS THE ENTIRE SPHERE SO THAT CHARGE NEUTRALITY IS CONSERVED, AS THIS IS THE MOST ENERGETICALLY FAVOURABLE ARRANGEMENT.

From Figure 21 it can be seen that the particles arrange themselves so that the absolute number of particles is almost exactly equal to the number of 'average mass particles'. This is to ensure that charge distribution is evenly spread across all the shells, which conserves charge neutrality (c.f. Figure 22). Varying the number of different masses, or their relative masses does not seem to change this relationship.

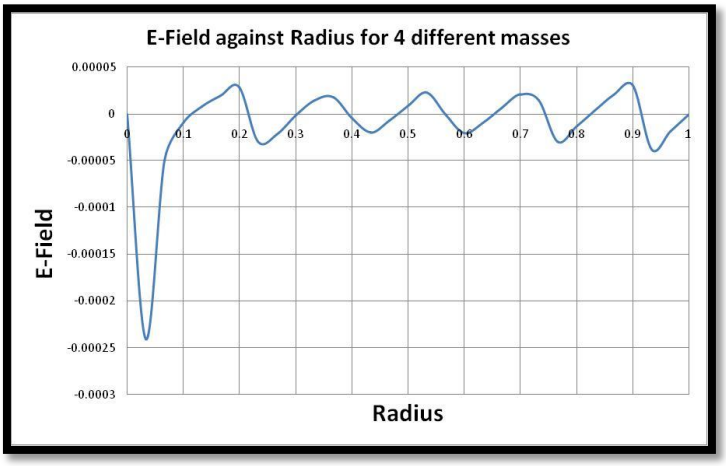

FIGURE 22 : SHOWING HOW THE E-FIELD IS WELL BALANCED EVEN WITH A VARIETY OF DIFFERENT CHARGE PARTICLES IN THE SYSTEM

The electric field shown in Figure 22 is almost identical to that found in Figure 5, although the system itself has very different parameters. Charge 'neutralization' is the key driving force behind the stability of the system. The stable point structures for the system are found to lie at the same values independent of the number of different mass/charge/radius particles within it.

HIGH PARTICLE NUMBER SIMULATIONS

Due to constraints of processor time it was not possible to run many very high number simulations apart from a few frames to check spherical distributions. Below is an example of a high particle number simulation. The data can currently not be verified because making sure the crystal has been given time to adjust and equilibrate would take an inordinate length of time. Only the box-tree coding or parallel processor support would allow these high N simulations to be investigated.

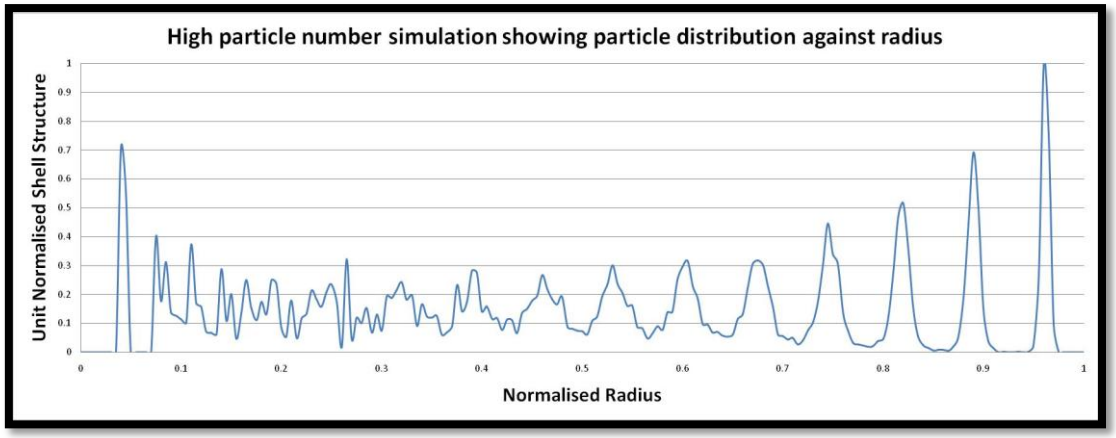

FIGURE 23 : THIS SIMULATION HAS 8691 PARTICLES WITHIN IT. AS USUAL THERE IS THE SHELL STRUCTURE WHICH CAN STILL BE SEEN FROM 1 – 0.3 RADII. HOWEVER, FROM 0 – 0.3 RADII A NEW NON-SHELL STRUCTURE IS OBSERVED.

From Figure 23 there is a distinct shift from shell structure far away from the edge and centre. This type of behaviour has been seen in 2-D simulations [18]. However, as explained after Figure 20 it requires an order of more particles to achieve this within a 3-D simulation. The graph above is by no means conclusive and stands alone, but further investigation into high N simulations would be highly beneficial.

By taking a z-slice of the new crystal it is apparent how the structure has re-ordered itself far from edge effects:

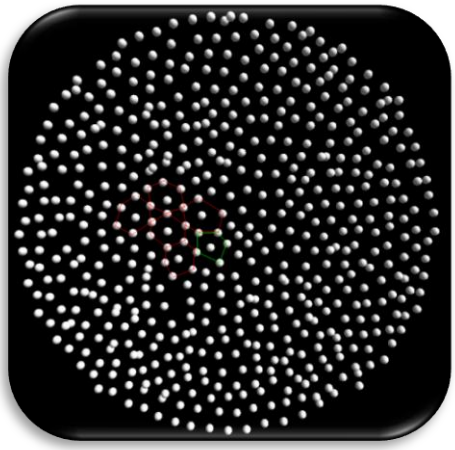

PICTURE 6 : A SCREEN CAPTURE FROM THE SIMULATION SHOWING HOW THE STRUCTURE APPEARS TO CHANGE FROM 'CONCENTRIC' CIRCLES TO A LESS SPHERICALLY BOUND STRUCTURE TOWARDS THE MIDDLE. NOTE THE RED/GREEN LINES SHOWING IRREGULAR HCP STRUCTURE.

Picture 6 still shows signs of a hexagonal structure towards the middle. However, without the bias towards the edges of the system it appears to have re-aligned itself. Due to time constraints it was not possible to run higher particle simulations, and because of the possible transitory nature (i.e. the crystal may still be affected by edge effects) there appear to be a lot of irregularities within the structure.

As discussed earlier the surface structure is hexagonally packed, but the volume packing efficiency is too low to qualify for true HCP structure. By plotting the volume packing efficiency (Number of particles enclosed within r, multiplied by the apparent volume each takes up then dividing by the total volume enclosed within r) the result for 8691 particles is shown in Figure 24 below on page 24.

$$\xi_{volume} = Packing\ Efficiency\ (Volume) = {N_d R_d^3}\Big/{R^3}$$

EQUATION 9 : WHERE R IS RADIUS AT R AND N_D IS NUMBER OF DUST PARTICLES WITHIN R.

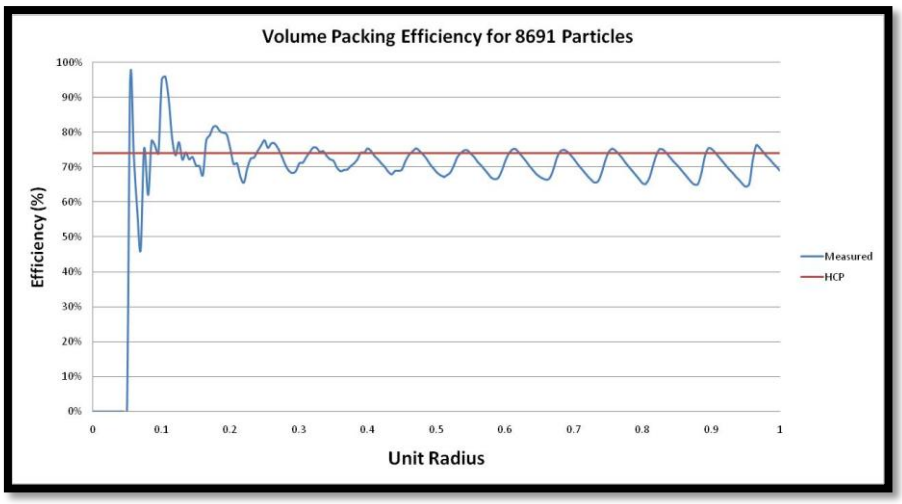

FIGURE 24: FOR A HCP STRUCTURE THE PACKING EFFICIENCY SHOULD BE 74% (RED LINE). NOTE THAT THIS GRAPH IS CUMULATIVE HENCE THE OVERALL VOLUME PACKING EFFICIENCY IS JUST UNDER 70%.

Towards the centre of the apparatus there is a definite increase in volume packing efficiency. Higher N simulations would need to be run to get an accurate estimate of the "new structure's" packing efficiency towards the centre of the apparatus. Towards the centre the sudden spikes are caused by single particles being out of place. When the volume is very small even a single particle can cause a massive change in volume packing efficiency. The simulation was then used to generate a HCP lattice of type (AB), where brackets denote repeating. There are three possible configurations used to stack spheres denoted A, B and C. (AB) is called HCP whereas (ABC) is called Face Centred Cubic.

"Relative to a reference layer with positioning A, two more positionings B and C are possible. Every sequence of A, B, and C without immediate repetition of the same one is possible and gives an equally dense packing for spheres of a given radius." [19]

The following density graph is output by the program for HCP:

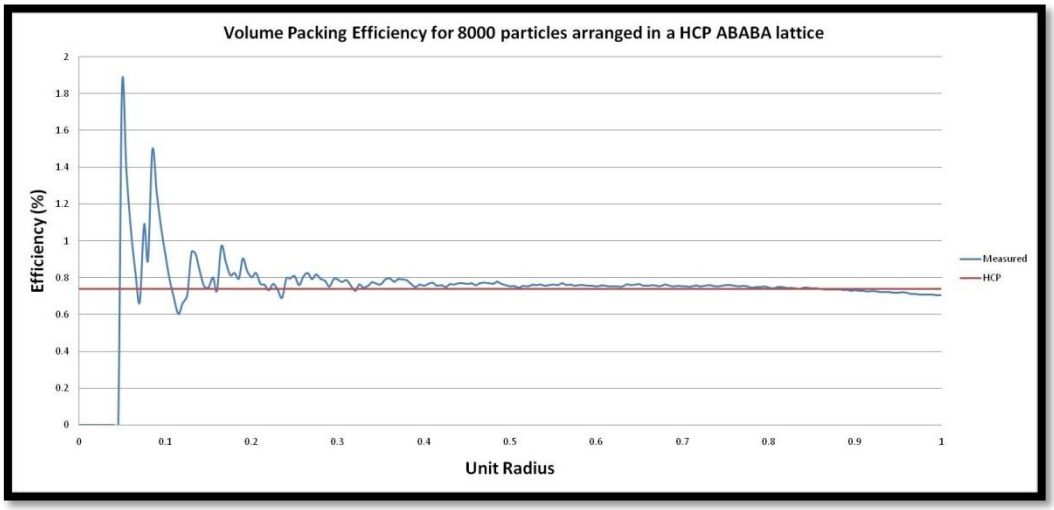

FIGURE 25: NOTE THAT EDGE EFFECTS CAUSE THE SLIGHT TAIL OFF AFTER ABOUT 0.9 RADII OUT AND THE SHARP SPIKES SEEN TOWRADS THE CENTRE OF THE APARATUS (THE HCP LATTICE DOES NOT QUITE OCCUPY THE ENTIRE VOLUME OF THE SPHERE). CLEARLY FROM APPROXIMATELY 0.5-0.9 RADII THE 74% PACKING EFFICIENCY IS VERY ACCURATE.

In a very high N simulation the pattern seen in Figure 25 above should be seen from the centre until about 10 particle radii away from the edge of the apparatus. Thereafter until the edge of the apparatus, the oscillating pattern observed in Figure 24 should be present due to edge effects.

OTHER INVESTIGATIONS UNDERTAKEN

Wave propagation within the dusty plasma crystal was also investigated by David Shone[12]. Waves were created through one of five processes:

1. Displacing an entire shell of particles outwards or inwards from the centre of the apparatus by varying amounts.
2. Displacing a few selected particles from one or more shells
3. Firing in particles from outside the apparatus (without conserving charge neutrality) and observing shock waves as the particle passes through the crystal.
4. *"Lateral Stretching"*, which is taking a slice through the centre of the crystal and radially displacing the entire slice section.
5. *"Probe Induced Oscillation"*, which is taking a charged probe and oscillating it inside or outside the apparatus.

Waves were *"measured to be 10±1 Debye lengths every 5±0.6 dust plasma periods"* [12]. Furthermore, when firing particles through the system Mach Cones were observed. Mach Cones are essentially a wake formed by a charged particle when it passes through the system. For a detailed discussion see David Shone's work [12].

ERRORS

COMPUTATIONAL

For our chosen Euler method there must be a careful consideration of the associated errors. There are four areas which must be addressed:

1. Consistency: The Euler method is consistent because if the step length were reduced to 0 then the true equation of motion would be reproduced.
2. Accuracy: Within accuracy there are four sources to consider:

    a) Truncation: Dependant on step length and the error is $O(h)^2$.
    $F = ma : F = m\frac{v}{t}\ or\ \frac{Fh}{m} = \Delta v.$
    b) Propagation: Because the system's energy is being actively controlled, the propagation error is minimal. If the system were left alone without any 'intelligent' cooling, the overall K.E. and total energy would gradually increase over time. The propagation error is not an issue as altering start conditions does not seem to affect the final outcome (c.f. Figure 10 and Figure 11 under the 'Stable Point investigation').
    c) Round off: IEEE Double Precision Standard has been utilised. 64 bits per value of which 52 form the mantissa thus the error is 15 standard deviations per calculation.
    d) Initial Conditions: See sub-heading 'Initial Condition Problem'.

3. Stability: The Euler method, unlike the leapfrog method is stable for decaying problems. As the simulation uses a small dissipative force to change CCP at all times the Euler method should be stable. Below are the conditions for stability for the Euler method:

$$|E_{n+1}| = g|E_n| \;\; Method\ stable\ for\ g \leq 1\ ;\ g\ is\ amplification\ factor$$

$$\left|\frac{|E_{n+1}|}{E_n}\right| = \left|1 + \frac{1}{m}\frac{\partial F}{\partial v}\mathrm{h} + O[(\mathrm{h})^2]\right|$$

$$g \leq 1 \;\Rightarrow\; -2 \leq \frac{1}{m}\frac{\partial F}{\partial v}\mathrm{h} \leq 0$$

4. Efficiency: The Euler method is among the fastest method requiring only one evaluation per step.

INITIAL CONDITION PROBLEM (ICP)

In any molecular dynamic simulation it is important not to start the simulation randomly [19]. If a simulation is started randomly some particles will be distributed too close to one another, leading to a spike in kinetic energy just after the start of the simulation. The spike is produced as a small fraction of the particles gain a massive increase in KE as they were placed too close together and rapidly push apart from one another. This leads to an inherent instability in the simulation which must be overcome.

After some time the system equilibrates and all the particles have increased KE. A Maxwell Boltzmann distribution of velocities is observed at this point, however the system has generally heated up sufficiently that the CPP will be in the region of approximately 2, even if particles are initialised with no thermal energy.

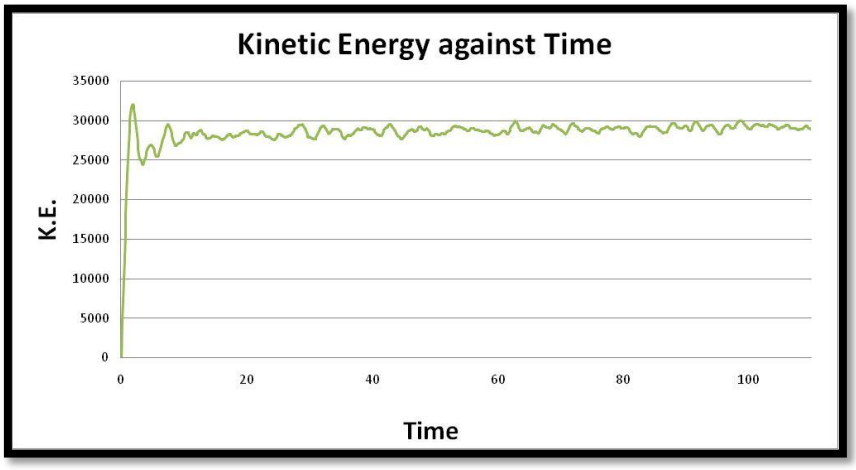

FIGURE 26 : SHOWING HOW THERE IS A MASSIVE SPIKE IN K.E. AT THE START OF ANY SIMULATION. THE SYSTEM THEN EQUILIBRATES AND STABILISES, WHICH CAN BE SEEN OCCURRING WITHIN ABOUT 15 PLASMA FREQUENCIES.

The solution to the ICP is to allow the system to equilibrate with the desired number of particles and then to gently cool the system down, removing the excess KE. The overall energy of the system even before the cooling process still resides in the massive potentials between the particles, so the overall energy of the system is altered only marginally through cooling the particles.

Once the particles have cooled down and crystallised their positions at time t and t-h (h is step length) are recorded. These 'crystals' of varying dust particulate numbers and charge are then saved and used for analysis on CCP variation.

EDGE EFFECTS

Edge effects are difficult to quantify accurately. It is clear that they do affect the structure and through investigation of high N simulations it should be possible to gauge how far within the sphere they propagate. Based on Figure 23 it can be assumed that there may be no more 'edge effects' 0.7±0.05 Radii away from the edge. The actual length of the radius was 349.026, thus 0.7 radii corresponds to 244±18 plasma Debye lengths, or about 10 particles 'in' until edge effects may become negligible. Particles cannot simply be moved away from the edge, they must be shielded by several layers of other particles.

OVERALL ERROR DISCUSSION

Taking all the above factors into consideration the overall system should be efficient and the overall errors should be very low, excluding edge effects, which are an unknown quantity. From the stable point analysis as well as multiple mass/charge/radius investigations it is very clear that the system manages to achieve the same results regardless of the makeup of the dust particles.

CONCLUSIONS

CURRENT INVESTIGATION

The current simulation is still a 'work in progress'. However, the results from the model seem to roughly match those predicted, such as the CCP phase change occurring at a value of 172. A further phase change seems to occur at a CCP of less than 1, which could be the liquid – gas phase change. Shell formations as well as shell stable points are of great interest, however due to a lack of time and data a proper numerical solution could not be reached in order to solve the problem of when the next stable point would occur. In conclusion edge effects seem to bias the structure towards spherically hexagonally packed lattices, but these 'shell' separations are not consistent with HCP structure. When large numbers of particles are used within a simulation approximately 10 shells in, a new structure, perhaps true HCP, is observed.

One of the most interesting aspects of the simulation is the occurrence of stable dusty plasma crystals for a large range of conditions through varying particle size, charge and radius. This has far reaching consequences as to how to minimise the 'damage' caused by these particles.

FURTHER INVESTIGATION

It is proposed that a box tree method should be utilised for the program so that high particle number simulations can be undertaken. The PCF should be modified so that only the middle 0-0.5 radii particles are used to calculate the PCF, which should result in the PCF tending to 1 rather than 0 with the current PCF function.

Furthermore it would also be highly beneficial to allow the program to use multiple processor threads so that dual and quad core processing power on PC's could be maximally utilised. To fully study edge effects it would be very useful to run the simulation in 2D. This could be achieved very easily. In 2D a factor of fewer particles are required to reach the same distance from the edge in comparison to 3D case, which would result in a far quicker processing time.

ACKNOWLEDGMENTS

I would like to thank the following for their contribution to the project:

- David Shone for keeping the project on track and reminding me why commenting is necessary for later understanding the code. Also for his massive help in doing the normalisations.
- Dr. M. Coppins and the PHD students in the Plasma physics group for their useful suggestions and willingness to hear our ideas and give feedback.
- James Yearsley and Sam Kitchen for helping devise the best fit line for stable points.

BIBLIOGRAPHY

[1]. **Shukla and Mamun.** *Introduction to Dusty Plasma Physics.* 2002.

[2]. **Wikipedia.** Plasma Physics. *Wikipedia.* [Online] [Cited: 24 September 2006.] http://en.wikipedia.org/wiki/Plasma_%28physics%29.

[3]. **Iowa Education Board.** Physics Today, July 2004. *Iowa Edu.* [Online] [Cited: 26 September 2006.] http://dusty.plasma.uiowa.edu/~goree/papers/PhysicsTodayJuly2004.html.

[4]. *Experimental Investigations of Dusty Plasmas.* **Merlino, Robert L.** Orleans : PACS 57.27.Lw, 2005. 4th International Conference on the Physics of Dusty Plasmas.

[5]. **Vasut, J A. and Hyde, T. W.** *Computer Modeling of Edge Effects in Plasma Crystals.* [E-Print] Lunar and Planetary Science XXXII : s.n., 2001. arXiv:physics/0401147.

[6]. *Plasma crystal: Coulomb crystallisation in a dusty plasma.* **Thomas, H. M. and Morfill, G. E.** 5, s.l. : Phys. Rev. Letters, 1994, Vol. 73, pp. 652-655.

[7]. *Coulomb solid of small particles iin plasmas.* **Ikezi, H.** 6, s.l. : Physics of Fluids, 06/1986, Vol. 29, pp. 1764-1766. 1986PhFl..29.1764I.

[8]. **Adachi, Satoshi.** *One Dimensional model of Self Organisation in Dusty Plasma.* s.l. : Japan Aerospace Exploration Agency, 2005. JAXA-RR-04-053E or ISSN 1349-1113.

[9]. **GNU.** GSL - GNU Scientific Library. *GNU.* [Online] 2007 February 2007. [Cited: 01 February 2007.] http://www.gnu.org/spftware/gsl/.

[10]. **Kilgard, Mark.** Nate Robins - Open GL. *XMission.* [Online] 8 November 1991. [Cited: 21 September 2006.] http://www.xmission.com/~nate/glut.html.

[11]. *Local simulations of planetary rings.* **Wisdom, J. and Tremaine, S.** pg 925-940, s.l. : Astronomical Journal , 03/1988, Vol. 95. ISSN 0004-6256.

[12]. **David, Shone.** *Investigating the Formation of Dusty Plasma Crystals and Related Phenomena using 3-D Molecular Dynamics Techniques.* 2007.

[13]. **Weisstein, Eric W.** Hexagonal Close Packing - MathWorld. *A Wolfram Web Resource.* [Online] 16 Febraury 2003. [Cited: 3 March 2007.] http://mathworld.wolfram.com/HexagonalClosePacking.html.

[14]. *Direct observation of Coulomb crystals and liquids in strongly coupled rf dusty plasmas.* **Chu, J. H. and I, Lin.** 25, s.l. : Phys. Rev. Lett., 1994, Vols. 72, 4009 - 4012. 10.1103/PhysRevLett.72.4009.

[15]. **Wikipedia.** Spherical Packing. *www.wikipedia.com.* [Online] 2006 December 2006. [Cited: 2007 March 11.] http://en.wikipedia.org/wiki/Sphere_packing.

[16]. *Ordering of dust particles in dusty plasmas under microgravity.* **Totsuji, Hiroo, et al.** s.l. : PHYSICAL REVIEW E, 14.04.05, Vol. 71. 045401.

[17]. **International Union of Crystallography.** Close-Packed Structures. *International Union of Crystallography.* [Online] 2 April 1998. [Cited: 14 March 2007.] http://www.iucr.org/iucr-top/comm/cteach/pamphlets/5/node0.html.

[18]. *Competition between Two Forms of Ordering in Finite Coulomb Clusters.* **Totsuji, Hiroo, et al.** 12, Okayama : Physical Review Letters, 03/2002, Vol. 88. id. 125002.

[19]. **Rapaport, D. C.** *The Art of Molecular Dynamics Simulation.* s.l. : Cambridge University Press, 2 edition (April 19, 2004). 0521825687 : 978-0521825689.

[20]. *Dusty Plasma Correlation Function Experiment.* **Smith, B and Hyde, Vasut T.** N/A, Houston : 34th Cospar Scientific Assembly, 02/2002, Vol. N/A. 2002cosp...34E.562S.

APPENDICES

APPENDIX A

Plasma Density, $n_p = 10^{15} m^{-3}$

Temperature of Electrons $T_e = \frac{2|e|}{k_B}$ *; i. e.* $2eV$

Electron Plasma Debye Radius: $\lambda_D = \sqrt{\frac{\varepsilon_0 k_B T_e}{n_p e^2}}$

Average charge (Z_d) *is user defined as is Gamma*(γ)

Temperature ratio, $T_{ratio} = \vartheta = \frac{Temp}{T_e}$ *where Temp is defined by the user at start of simulation.*

Average Inter-particle Distance, $Intr = R_{int} = \frac{{Z_d}^2}{3.0\gamma\vartheta N}$ *where* $N = \frac{4\pi{\lambda_D}^3 n_p}{3}$*; N = number of electrons in Debye sphere*

Radius of Apparatus $R_a = R_{int} \times \left\{\frac{3\times Particles}{4\pi}\right\}^{\frac{1}{3}}$

Number Density $n = \frac{Particles}{N{R_a}^3}$

Thermal Velocity $V_{th} = \sqrt{\frac{k_B T_e}{m_e}}$ *and Mach speed* $M(Mach\ Number) = \frac{v}{v_{th}}$

Gamma (Normalized) $\gamma = \frac{{Z_d}^2}{3R_{sep}\theta N}$

$E_{gauss}^{Norm}(r) = \frac{\sum_{R=0}^{R=r}(dust\ charge\ and\ plasma\ charge)}{3Nr^2}$*; The Sum part simply sums every charge between the centre of the simulation and the distance out where the electric field is being measured. The E-field is set to 0 at r=R.*

Potential $V_{plasma}^{Norm} = \frac{Z_{tot}}{2NR_a}\left\{1 - \frac{R_{sep}^2}{3R_a^2}\right\}$

E-Field $E' = \frac{Ee\lambda_0}{k_B T_e}$ *where E is un-normalised electric field*

E-Field from plasma $E'_{plasma} = \frac{Z_{tot}R}{3NR_a^3}$ *at distance R from centre*

E-Field between particles $E'_{part} = \frac{Z}{3NR_{sep}^2}$

Normalised mass was normalised to the mass of an electron.